Unconventional Superconductivity at Mesoscopic Point-contacts on the 3-Dimensional Dirac Semi-metal Cd_3As_2

by

Abhishek Gaurav

A dissertation submitted for the partial fulfilment of
BS-MS dual degree in Science

in
Department of Physical Sciences

INDIAN INSTITUTE OF SCIENCE EDUCATION AND RESEARCH, MOHALI

April 2015

Certificate of Examination

This is to certify that the dissertation titled Unconventional Superconductivity at Mesoscopic Point-contacts on the 3-Dimensional Dirac Semi-metal Cd_3As_2 submitted by Mr. Abhishek Gaurav (Reg. No. MS10037) for the partial fulfilment of BS-MS dual degree programme of the Institute, has been examined by the thesis committee duly appointed by the Institute. The committee finds the work done by the candidate satisfactory and recommends that the report be accepted.

Dr. Sanjeev Kumar	Dr. Yogesh Singh	Dr. Goutam Sheet (Supervisor)

Dated: April 25, 2015

Declaration

The work presented in this dissertation has been carried out by me under the guidance of Dr. Goutam Sheet at the Indian Institute of Science Education and Research Mohali. This work has not been submitted in part or in full for a degree, a diploma, or a fellowship to any other university or institute. Whenever contributions of others are involved, every effort is made to indicate this clearly, with due acknowledgement of collaborative research and discussions. This thesis is a bonafide record of original work done by me and all sources listed within have been detailed in the bibliography.

Abhishek Gaurav
(Candidate)
Dated: April 25, 2015

In my capacity as the supervisor of the candidates project work, I certify that the above statements by the candidate are true to the best of my knowledge.

Dr. Goutam Sheet
(Supervisor)

Acknowledgements

I would like to thank my supervisor Dr.Goutam Sheet for providing me the opportunity to work under his supervision. I thank him for introducing me to the exciting phenomenon of superconductivity and its realization through experiments in the lab. He introduced me to different techniques which includes the Point Contact Spectroscopy, a wonderful technique for probing the superconductors and ferromagnets. I was introduced to Labview and Solidworks....due credit goes to him as an instructor in the Advance Electronics Lab during my 6^{th} *semester. I love these two tools which have been useful throughout in interfacing instruments and in preparing computer aided drawing.*

I thank Mr.Avtar Singh who helped in running the lab and the liquid Helium plant smoothly and making things readily available. We hardly ran out of liquid Helium during the experiments. I take this opportunity to thank Jithin, a friend and a motivator. I consider him as an electronics wizard.. who could do things out of no where, his ideas were full of 'juggad'(innovation). He was a well known programmer in the campus and I was often benefited.

I thank Mr.Gohil S Thakur, Zeba Haque and Prof.A K Ganguly for providing us the Cd_3As_2 *sample and its intial characterization. I duly acknowledge the contribution of Ashwini, Kavita and Dr. Yogesh Singh for the VSM and the resitivity measurement. I thank my collaborator Ms. Leena Aggarwal for taking up the project together on* Cd_3As_2 *and working on the manuscript together. I also thank all my labmates who at times would happily help in various tasks in the lab. Due credit goes to Shekhar, Aslam, Preetha, Shubhra, Amit Ji and Anshu.*

I thank my buddies Imran and Shivam who were always with me...we shared our happiness and sorrow. I thank all of you...Upakul, Nitish(CM), Pratip, Jagdish and Yogesh for being together all the five years. Irfana, Reshma, Asha ...you will be missed. Anshu...I thank you for being such a nice person.

Li'l Piku...Abhishek will miss you. We had so much of fun together.

I thank IISER Mohali for accommodating me during the five years of my BS-MS and my family for the constant support. Thanks to DST INSPIRE for partial financial support. Finally, I thank my Mom for having the courage to let her only son explore .... I love you Mom.

Contents

List of Figures

List of Tables

Physical Constants

Speed of Light $c = 2.997\ 924\ 58 \times 10^{8}\ \mathrm{ms}^{-\mathrm{S}}$ (exact)

Electron rest mass $m_e = 9.10938291 \times 10^{-31}\mathrm{kg}$

Lorentz number $L \approx 2.45 \times 10^{-8}\mathrm{V}^2/\mathrm{K}^2$

Reduced Planck constant $\hbar = 1.054571726 \times 10^{-34}\mathrm{Js}$

For Bond44

Abstract

by Abhishek Gaurav

Three dimensional (3D) Dirac semi-metals(DSs), a recently proposed state of quantum matter and bulk analogue of graphene exist close to topological phase-boundaries and there exists possibility of driving them into exotic phases (such as topological superconductors, Weyl semi-metals, axion insulators) by breaking certain symmetries. Cd_3As_2 is a model 3D DS, ideal for the realization of such exotic phases. However, a practical realization of this idea was lacking. Here by implementing the Point Contact Spectroscopy we show that the mesoscopic point-contacts between pure silver (Ag) and the 3D DS Cd_3As_2 exhibit unconventional superconductivity with a critical temperature (on- set) more than 6 K. The phenomenon reported here is unique since none of Cd_3As_2 or Ag is a superconductor. A gap amplitude of 6.5 meV is measured spectroscopically in this phase that varies weakly with temperature and survives up to a remarkably high temperature of 13 K indicating the presence of a robust normal-state pseudogap. The observations indicate the emergence of a new unconventional superconducting phase that exists in a quantum mechanically confined region under a point-contact between a Dirac semi-metal and a normal metal.

Chapter 1

Introduction

1.1 3D Dirac semi-metals

Solids are divided into metals or insulators depending whether there exists a finite bangap or not. Insulators can be further categorized into normal or topological insulator[1, 2] based upon the topology of their electronic structure. A three dimensional (3D) Dirac semi-metal(DS)[3] is a distinct class of electronic material in which the conduction band and the valence band touch each other at single, discrete points in k-space, around which the dispersion is linear in k. Thus DS can be visualized as a true 3D analogue of graphene. The unusual dispersion relation makes the electron around the Fermi energy to behave like highly realativistic particles unlike non-relativistic Schrodinger particles in metals and semi-metals. Unlike 2D Dirac fermions in graphene a 3D DS possesses bulk Dirac fermions. Examples of DSs include $\mathrm{TlBiSe}_{2-x}\mathrm{S}_x$, $\mathrm{Na_3Bi}$[4], $\mathrm{Cd_3As_2}$[5] etc.

$\mathrm{Cd_3As_2}$ has been recently shown to have a pair of 3D Dirac fermions by angle-resolved photoemission spectroscopy experiment. A crytallographic cell of $\mathrm{Cd_3As_2}$ comprises of intercalated face-centred cubic(fcc) arsenic sublattice and a cadmium sublattice with two vaccancies as shown in Figure 1.1[5].

1.2 Point Contact Spectroscopy

A point contact(PC) stands for a contact between two substance over a very small area[6]. The area of such point contact is lower bound by the interatomic

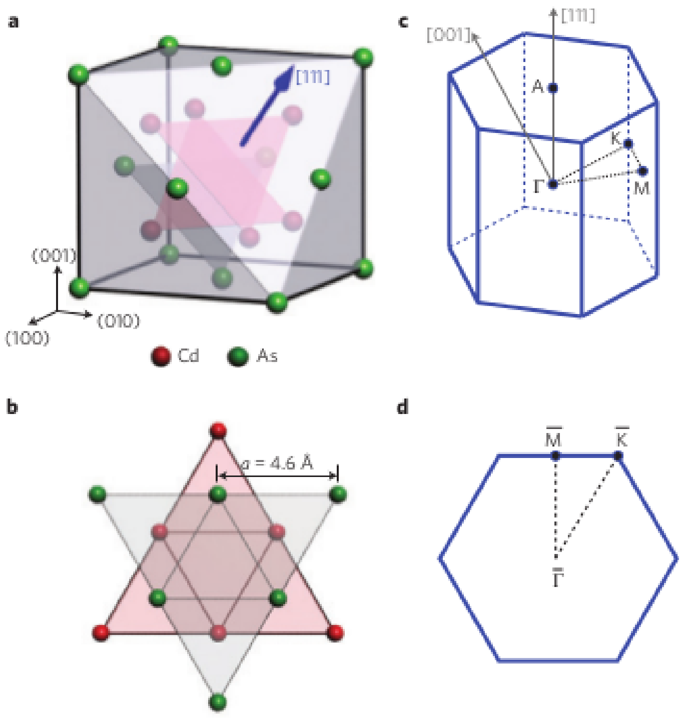

Figure 1.1: (a) Crystal structure of Cd$_3$As$_2$, showing an intercalated Cd cubic lattice (with two vacancies) inside the fcc As lattice. The blue arrow indicates the normal of the (111) surface, where the crystal naturally cleaves. (b) Projected view of the lattice along the [111] direction, showing the stacking As and Cd layers with in-plane lattice constant a = 4.6 . (c) Bulk Brillouin zone of Cd3 As2 (111) with high-symmetry points indicated. Grey arrows indicate the [001] and [111] directions, respectively. (d) Projected surface Brillouin zone in the kx ky plane. Figure taken from [5]

distance in solid and can be as large as one μm. Due to surface irregularities or coatings(oxide layer or other compound adsorbed on the surface) the true area of contact is always lower than the total mechanical contact between the two substances forming the point contact. The point contact that we are dealing with, ranges from few tens to hundreds of nanometer.

Voltage-Current(VI) characteristic of narrow constrictions like the one formed by PCs between two metals deviates from the Ohm's law. The scattering mechanism of the electrons and other elementary excitation can be derived from the study of its characteristics under the applied voltage, which limits the energy of the undergoing interactions. Point Contact Spectroscopy **(PCS)** is a method for the study of elementary excitation spectra in conductive solids with the aid of PCs.

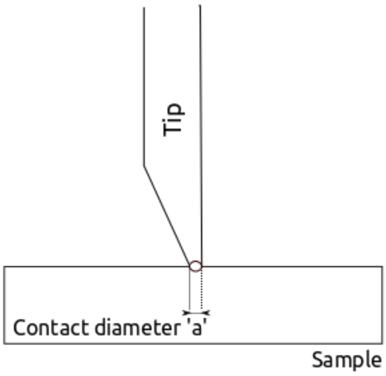

FIGURE 1.2: Point Contact schematic showing the formation of PC at the interface of a tip and sample

The scattering within a PC depend on the size of the PC itself and the transport through such PC can be divided into different regimes depending upon the ratio of the point contact diameter (a) to the mean free path(l) of the electrons. If the elastic a is much smaller than l then the electrons do not undergo any scattering within the PC statistically. Such contact are said to be in **ballistic regime** of transport. The resistance of PC in this regime is independent of the bulk resistance and is known as Sharvin's resistance[7, 8] or $R_S = \frac{2h}{e^2(ak_F)^2}$, where k_F is the Fermi momentum. Both momentum and energy of the electron is conserved when an electron passes through a ballistic regime. The electrons dissipate energy away from the contact region. When a becomes sufficiently small comparable to the de-Broglie wave length of the electron the ballistic regime turns into quantum regime where conductance quantization is observed.

On the contrary the when a is sufficiently larger than the inelastic l then the electrons dissipate energy in the contact regime itself and the contact is said to be in **thermal regime**. The resistance in this regime is given by Maxwell's Resistance or $R_M = \frac{\rho}{2a}$. Due to the Joule heating in the contact region itself the local temperature of the contact region increases and is given by $T_{eff}^2 = T_{bath}^2 + \frac{V^2}{4L}$ where L is the Lorentz number and V is the applied voltage. For an increase in 1 mV the sample temperature would increase by 3.2 K[9]. Such contact heating prevents the spectroscopic measurement of the contact in the thermal regime as the information gets killed due to overheating of the PC.

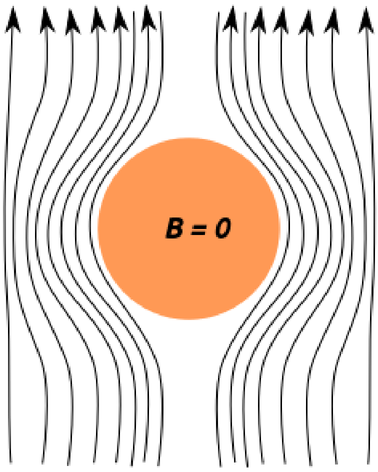

Figure 1.3: A conventional superconductor showing perfect diamagnetism below T_C

1.3 Superconductivity

Materials showing zero resistance and perfect diamagnetism below a certain temperature(known as critical temperature T_C)are classified as superconductors and the phenomenon is known as superconductivity. The formation of Cooper pairs by the pairing electrons below T_C gives rise to this novel phenomenon. Superconductors with low T_C are theoretically covered under BCS[10] formalism and said to be **conventional superconductors**. BCS formalism accounts for the attracting potential responsible for the formation of Cooper pairs. An electron interacting with the lattice due to Coulomb attraction, causes lattice deformation which in turn causes another electron in its vicinity get attracted to the electron. The two electrons under attraction have opposite momenta **k** and -**k** and are symmetric under exchange of positions. The spins take care of the Fermionic property of the combining electrons under exchange. Owing to the isotropic nature of electron-phonon interaction the BCS superconductors are called s-wave($L = 0$) superconductors. The minimum energy required to break a cooper pair is called the superconducting energy gap Δ.

The weaker attractive potential responsible for the formation of Cooper pairs can also originate due to other mechanism apart from the electron-phonon interaction as in the case of the conventional pairing. Magnetic interactions like ferromagnetic and antiferromagnetic spin fluctuations may also favor Cooper pair formation[9]. In such cases the Δ is anisotropic in **k**. For example antiferromagnetic fluctuations give rise to Cooper pairs in high T_C superconductors where Δ

have a $d-$wave symmetry($L = 0$). Similarly in case of spin triplet($S = 1$) superconductor like Sr_2RuO_4 ferromagnetic fluctuations lead to Cooper pairing and the order parameter have a $p-$wave symmetry. Superconductors with anisotropic gap(which changes its phase with the direction of $\mathbf{k}$) are known as **unconventional superconductors**.

1.3.1 Bogoliubons

The elementary quasi-particle excitations in superconductors are called *Bogoliubons*[10]. These quasi-particles exist only in the excited state and the minimum energy required to excite them equals $\Delta(\mathbf{k})$. The creation and anhilation of Bogoliubons are given in terms of the creation and anhilation of electrons as

$$c_{\mathbf{k}\uparrow} = u^*_{\mathbf{k}}\gamma_{\mathbf{k}0} + v_{\mathbf{k}}\gamma^*_{\mathbf{k}1} \tag{1.1}$$

$$c^*_{-\mathbf{k}\downarrow} = -v^*\gamma_{\mathbf{k}0} + u_{\mathbf{k}}\gamma^*_{\mathbf{k}1} \tag{1.2}$$

where the numerical coefficients satisfy $|u_{\mathbf{k}}|^2+|v_{\mathbf{k}}|^2 = 1$. $|v_{\mathbf{k}}|^2$ and $|u_{\mathbf{k}}|^2$ respectively are the probability of occupation and de-occupation of the pair($\mathbf{k}\uparrow$,$-\mathbf{k}\downarrow$). $\gamma_{\mathbf{k}0}$ destroys an electron with $\mathbf{k}\uparrow$ or creates one with $-\mathbf{k}\downarrow$ and have a net effect of decreasing the system momentum by $\mathbf{k}$. The operator $\gamma^*_{\mathbf{k}1}$ has similar properties and has a net effect of increasing the momentum by $\mathbf{k}$.

In position representation the electron-like and the hole-like wave-function of quasi-particles can be written as

$$\Psi_{e-like} = \begin{pmatrix} u \\ v \end{pmatrix} e^{iqx} \tag{1.3}$$

$$\Psi_{h-like} = \begin{pmatrix} v \\ u \end{pmatrix} e^{-iqx} \tag{1.4}$$

where, $u^2 = \frac{1}{2}[1 + \frac{(E^2-\Delta^2)^{1/2}}{E}] = 1 - v^2$

1.4 Point Contact Andreev Reflection or PCAR

The phenomenon of Andreev reflection occurs when an electron from a normal metal tries to enter a superconductor but gets reflected as a hole with opposite

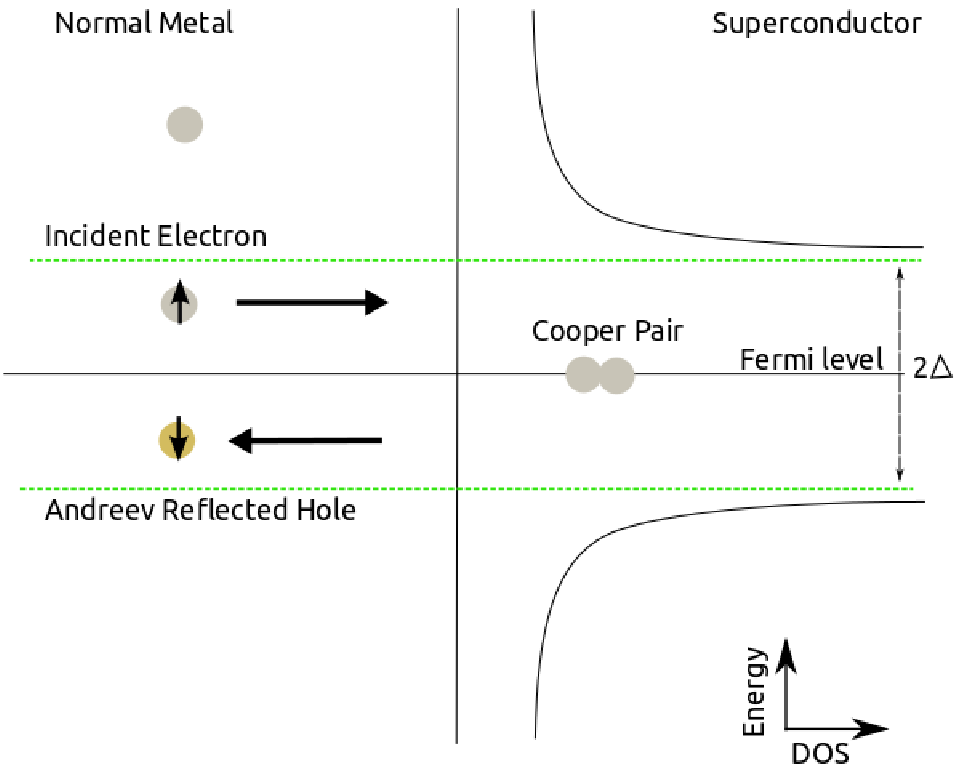

FIGURE 1.4: Schematic of Andreev reflection through a N-S interface

spin when it encounters the superconducting energy gap[9]. Subsequently a Cooper pair propagates through the superconductor and normal current gets converted into supercurrent. As shown in the figure if electron energy is higher than the superconducting energy gap Δ, then it gets transmitted into the superconductor. However for electrons having energy less than Δ gets Andreev reflected.

Andreev reflection is analysed using the normalized spectrum of conductance $\frac{G(V)}{G_N(V)}$ as a function of applied voltage V, where $G = \frac{dI}{dV}$ and $G_N = \frac{dI}{dV}$ at $V >> \frac{\Delta}{e}$

1.4.1 PCAR spectrum analysis

PCAR spectrum are analyzed in framework of Blonder-Tinkham-Klapwijk or BTK[11] theory. This theory models the interface between the normal metal and the superconductor as a delta function potential of the form $H = V_0.\delta(x)$ at $x = 0$ and is mathematically characterized by a dimensionless parameter $Z = \frac{V_0}{hv_F}$. Z arises due to Fermi vector mismatch between the two electrodes or due to the insulating barrier at the interface. Z can never be zero due to Fermi vector mismatch and henceforth there is always a normal reflection (with probability $B(E)$) apart from the Andreev reflection (with probability $A(E)$). The current through the N-S junction is given by

$$I_{N-S}N(0).v_F \int_{-\infty}^{+\infty} [f_0(E-eV) - f_0(E)][1 + A(E) - B(E)]dE \tag{1.5}$$

where $N(0)$ is the density of state at the Fermi level and v_F is the Fermi velocity. The probability as a function of the barrier was found by solving Bogoliubov equations(given below).

$$i\hbar\frac{\partial f}{\partial t} = [\frac{-\hbar^2\bigtriangledown^2}{2m} - \mu(x) + V(x)]f(x,t) + \Delta(x)g(x,t) \tag{1.6}$$

and

$$i\hbar\frac{\partial g}{\partial t} = [\frac{-\hbar^2\bigtriangledown^2}{2m} - \mu(x) + V(x)]g(x,t) + \Delta(x)f(x,t) \tag{1.7}$$

Where, $\Delta(x)$ is the gap, $\mu(x)$ is the chemical potential $f(x,t)$ and $g(x,t)$ are the element of BCS quasistate

$$\Psi = \begin{pmatrix} f(x,t) \\ g(x,t) \end{pmatrix} \tag{1.8}$$

and are proportional to u and v.
The trial solution keeping $\mu(x)$,$V(x)$ and $\Delta(x)$ constant are taken to be

$f = ue^{(ikx-iEt)/\hbar}$ and $g = ve^{(ikx-iEt)/\hbar}$
For $V = 0$,

$$E = \sqrt{[\frac{\hbar^2k^2}{2m} - \mu]^2 + \Delta^2} \tag{1.9}$$

For $E > 0$,

$$u^2 = \frac{1}{2}[1 \pm \frac{(E^2-\Delta^2)^{1/2}}{E}] = 1 - v^2 \tag{1.10}$$

The incident, reflected and transmitted wave-functions are given by

Incident electron: $\begin{pmatrix} 1 \\ 0 \end{pmatrix} e^{ikx}$

Normally reflected electron: $\begin{pmatrix} 1 \\ 0 \end{pmatrix} e^{-ikx}$

Co-efficeient	$E < \Delta$	$E > \Delta$
$A(E)$	$\frac{(\Delta/E)^2}{1-\epsilon(1+2Z^2)^2}$	$\frac{(uv)^2}{\gamma^2}$
$B(E)$	$1 - A(E)$	$\frac{[u^2-v^2]Z^2(1+Z^2)}{\gamma^2}$

Table 1.1: Reflection coefficient for Andreev and normal reflection calculated using BTK theory with $\gamma^2 = [[u^2 - v^2]Z^2 + u^2]^2$ and $\epsilon = \frac{(E^2-\Delta^2)}{E^2}$

Andreev reflected electron: $\begin{pmatrix} 0 \\ 1 \end{pmatrix} e^{ikx}$

Total reflected wave-function: $a \begin{pmatrix} 0 \\ 1 \end{pmatrix} e^{ikx} + \begin{pmatrix} 1 \\ 0 \end{pmatrix} e^{-ikx}$

Transmitted Cooper pair: $c \begin{pmatrix} u \\ v \end{pmatrix} e^{iqx} + a \begin{pmatrix} v \\ u \end{pmatrix} e^{-iqx}$

The appropriate boundary condition using the wave function in the normal metal Ψ_N and in the superconductor Ψ_S can be laid down as:

1. The continuity of Ψ's across the interface given by $\Psi_N = \Psi_S = 0$ at $x = 0$
2. The discontinuity of the first derivative of the Ψ's given by $\Psi_S - \Psi_N = \frac{2m}{\hbar} V_0 \Psi_N$ at $x = 0$

The application of the above boundary conditions along with the assumption that the Fermi velocities are equal i.e. $k = q = k_F$ leads the the probabilities a^*a and b^*b to values tabulated below.

If the Fermi vector mismatch is considered across the interface then the Z gets modified and is given by $Z_{eff}^2 = Z^2 + \frac{(r-1)^2}{4r}$ where $r = \frac{k}{q}$ and is the ratio of the Fermi velocity in normal metal to the Fermi velocity in superconductor. For practical $N - S$ interface $r \neq 1$ which makes Z_{eff} finite even in the absence of any insulating barrier[9]. The simulation below describes spectra in for different T, Δ and Z.

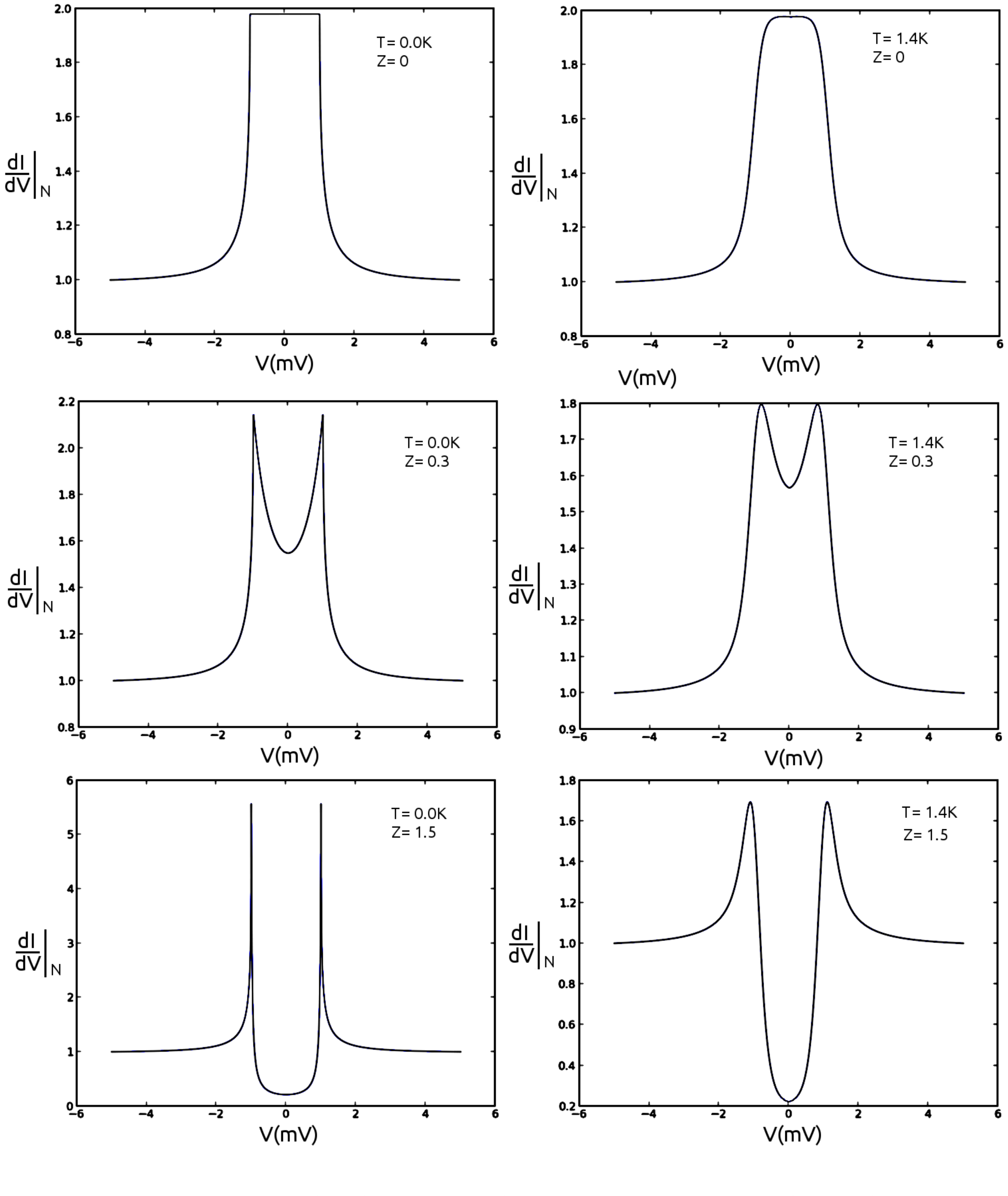

Figure 1.5: BTK simulated spectra with respective parameters.The conductance doubles in absence of any insulating barrier($Z = 0$)

Chapter 2

Synthesis and Characterization

2.1 Material Synthesis

Polycrystalline sample of Cd_3As_2 was obtained by using a powder mixture in stoichiometric ratio of Cd and As(1 gram) sealed in an evacuated quartz tube(10^{-5} mabar), furnace heating the tube at 500 °C for 8 hours followed by 24 hours of heating(with a ramp rate of 1 deg C) at 800 °C and finally cooling down the sample inside the furnace to room temperature. The shiny black crystalline product thus obtained was ground well and pelletized. The pellet was heated at 400 °C for homogenization and a shiny black and hard pellet of Cd_3As_2 was obtained.

2.2 X-Ray Diffraction

It is one of the most useful technique for the characterization of the solid samples and works on the priciple of Bragg diffraction by the atomic planes in the material. According to Bragg's law $n\lambda = 2d\sin(\theta$, where n is the order of diffraction, d is the distance between the atomic layers and θ is the angle of diffraction. In diffraction pattern peaks appear at θ appear for each of the d values. Bruker D8 Advance diffractometer was used for the characterization of the sample by X-ray diffraction(using Cu-Kα λ =1.506Å radiation). The peaks were indexed on the basis of tetragonal cell in $I4_1$ space group as reported by Cava et. al. Lattice parameters calculated using $Le'Bail$ method were in close agreement with the

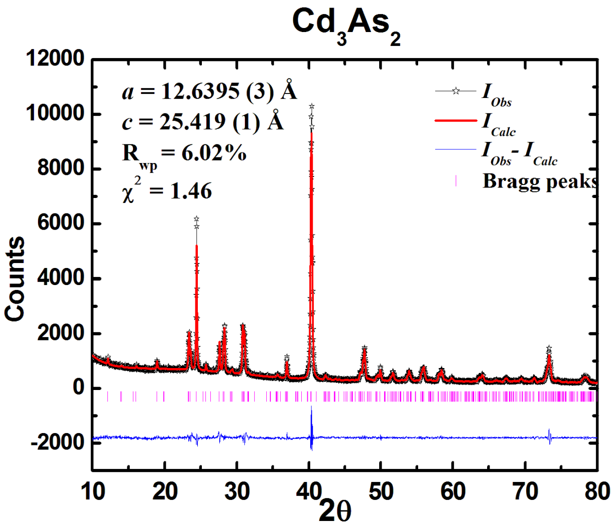

FIGURE 2.1: Powder x-ray diffraction pattern of polycrystalline Cd3 As2 fitted with LeBail. The vertical bars indicate the allowed Bragg reflections.

literature values. Thus using X-ray diffraction analysis the sample was found to be pure with no apparent impurity.

2.3 Energy Dispersive X-ray analysis(EDAX)

The elemental composition of the materials can be checked by measuring the energy corresponding to a particular emission or absorption. EDAX works in close conjugation with SEM which is use to bombard electrons on the atomic shells of the materials. Some of the inner shell electrons are knocked out and eventually outer shell electrons occupy the vacant inner shells by giving up energy as X-rays. Measuring the amount of energy present in the X-rays, the identity of atom present in the material can be established. The concentration of the specimen is judged based on the intensity of the particular X-ray peak in the EDAX spectrum. The analysis of the composition of Cd_3As_2 was tested using a SEM-EDAX. The average stoichiometry over different region of the sample was found close to 3:2(Cd:As). Some regions of the sample was found to be As deficient. The presence of C and Si in the image is due to the carbon tape and the detector respectively.

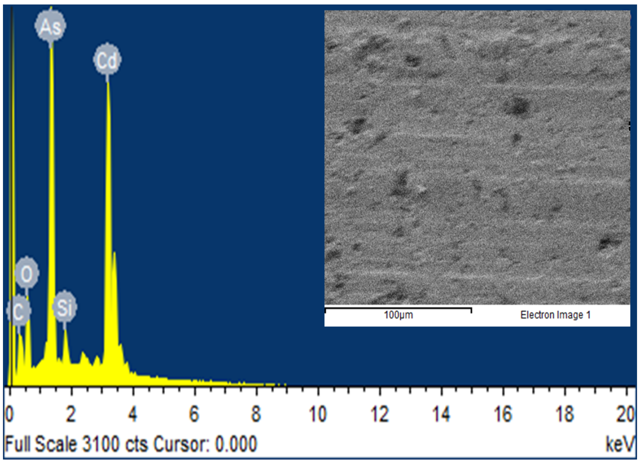

Figure 2.2: EDAX spectrum of Cd3 As2 . The inset shows image of polished pellet of Cd3 As2 .

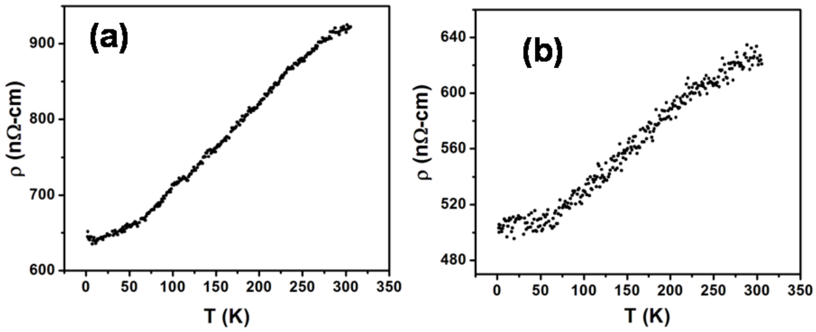

Figure 2.3: Raw data for four probe resistance vs. temperature of three bulk Cd3 As2 samples with varying mobility. All three of them lead to the new superconducting phase in a point-contact geometry.

2.4 Four Probe Resitivity Measurement

Four probe resitivity of the sample was measured using Quantum Design PPMS. Four linear contacts were made on the sample using silver epoxy and gold wires and the sample was mounted on the puck which was then transferred to the PPMS for the measurement. The sample shows semi-metallic behavior. Clearly it doesn't show any superconducting transition. Four probe resitivity has the advantage of giving very accurate result as the contact resistance doesn't come into picture (the voltage probes are away from the current leads and draw negligible current).

2.5 Magnetization of the Bulk Sample

To check the possibility of the hidden superconducting phase, the Vibrating Sample Magnetometer(VSM) experiment was done. The measurement was performed at a field of 100 Oe in a Quantum Design PPMS using a VSM probe. The magnetization didn't show any diamagnetic transition down to 2K.

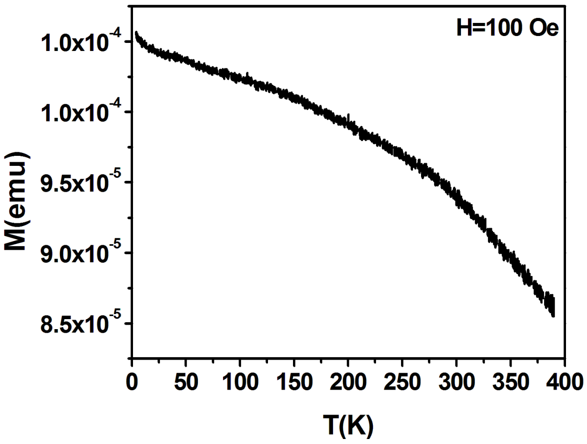

FIGURE 2.4: Magnetization vs. temperature of the bulk sample measured in a VSM in a Quantum Design PPMS. The bulk sample does not show any diamagnetic transition at low temperature down to 2 K.

Chapter 3

Tools and Techniques

3.1 Instrumentation and Measurement

The figure below describes the measurement technique used for acquiring the PCS spectra. An ac-modulation technique is used to record the differential resistance as a function of applied voltage. In this technique a small ac signal is coupled to the dc current which is swept in a certain range. The ac and dc voltage across the PC were measured using a lock-in amplifier(SRS830) and a digital multimeter(Keithley 2000 DMM).

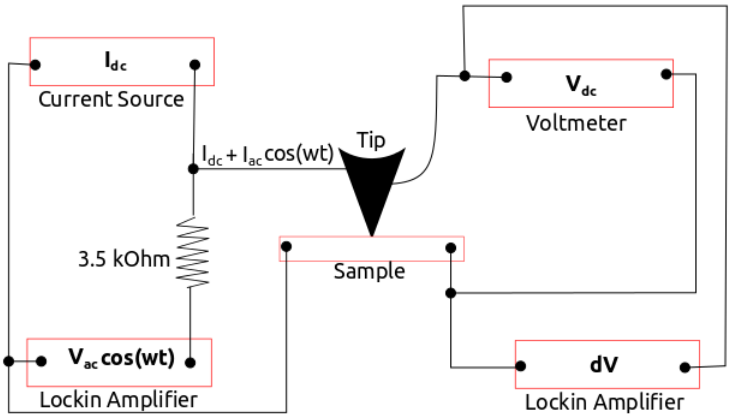

FIGURE 3.1: Schematic for recording point contact spectra using an ac modulation technique

3.1.1 PCS probe and point-contact fabrication

All the measurements were taken using a home-built point contact probe. The probe has space for mounting the tip and to which twisted pair of copper wires run from the top along the length of the probe. The sample space also houses a cartridge heater and a Cernox temperature sensor, used for controlling the temperature. The probe can be vacuum sealed once it gets inserted into the cryostat through a KF40 flange. The cryostat has been custom designed to meet the experimental requirements and have been manufactured by the American Magnetics Inc. The cryostat houses a 3-axis superconducting vector magnet with a magnetic field of 6T in the vertical direction. The cryostat has a 75 litres liquid He capacity and is facilitated by the central Liquid Helium Plant at IISER Mohali. The probe goes inside a static Variable Temperature Insert(VTI) which in turn is housed inside a dynamic VTI. The dynamic VTI lets the temperature go further down from 4.2K to 1.4K by pumping on the liquid He sipping through a controlled capillary dipped in the liquid He outside the dynamic VTI. The sudden expansion of the liquid He cools down the Helium by the process of Joules-Thomson expansion.

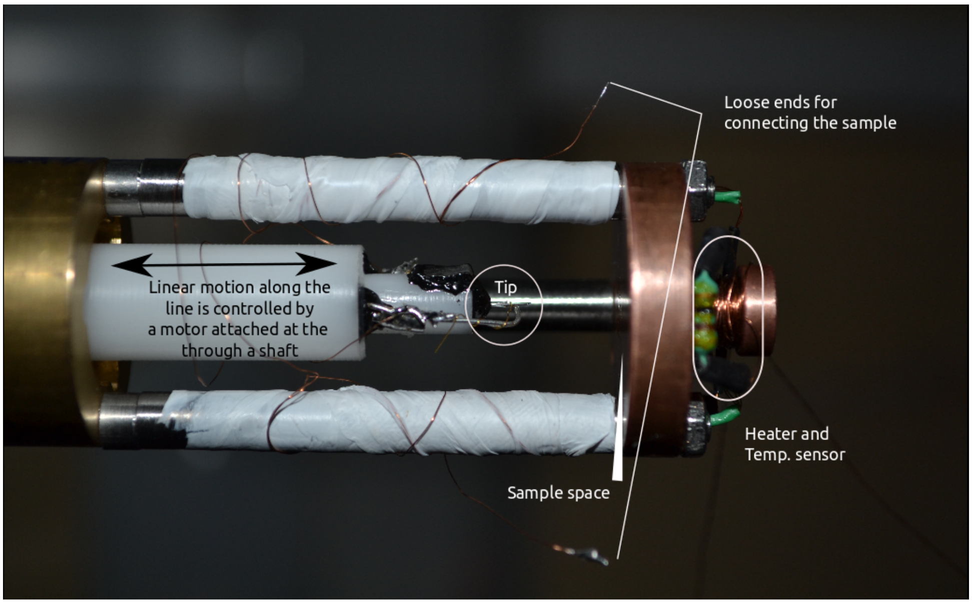

FIGURE 3.2: The lower end of the PCS probe that was used for the measurement.

Of the various known method of creating a PC, we use the needle-anvil method. In this method a sharp metallic tip is pressed into the sample to create a PC at the interface. The size of the PC is controlled by a 100 turns/inch stepper motors which rotates the shaft to create a linear

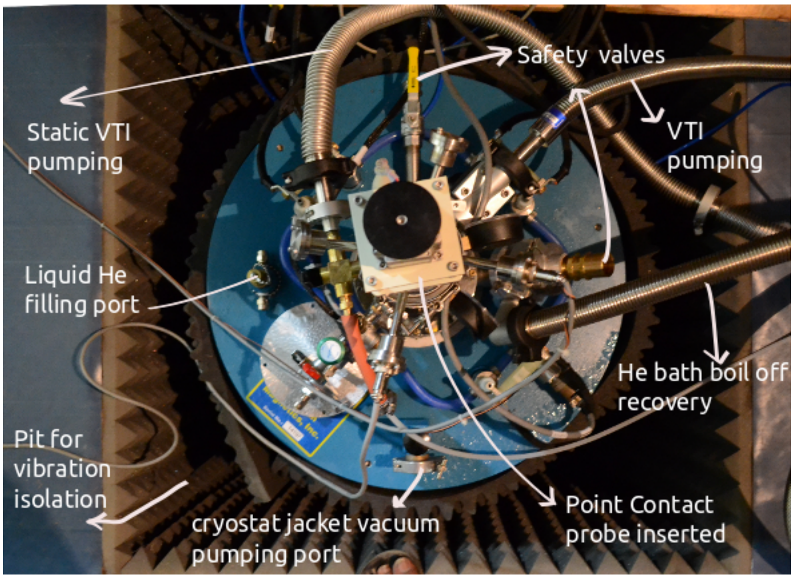

3.2 Data Acquisition Programs

The data acquisition programs were written in house using Labview. During my thesis various programs were developed for data acquisition and controlling the instrument. The following subsection summarizes my attempt.

3.2.1 The Temperature Control Program

One of the main task while running the experiment was to control the temperature at which the experiment is being performed. Some times the experiment required to ramp-up or ramp down the temperature at a specific rate.The program was written for a Lakeshore350/335 temperature controller and is capable of controlling the sample as well as the VTI temperature.

3.2.2 The RT Program

The Resistance Vs. Temperature(RT) program was written for acquiring the resistance as a function of temperature of the sample. The program takes the voltage across the sample measured using a SRS830 lock-in amplifier and plots it against the temperature recorded using the Lakeshore temperature controller. Another version of this program is capable for recording the RT of two samples simultaneously using two lock-in amplifiers. The data acquired are written in separate text files.

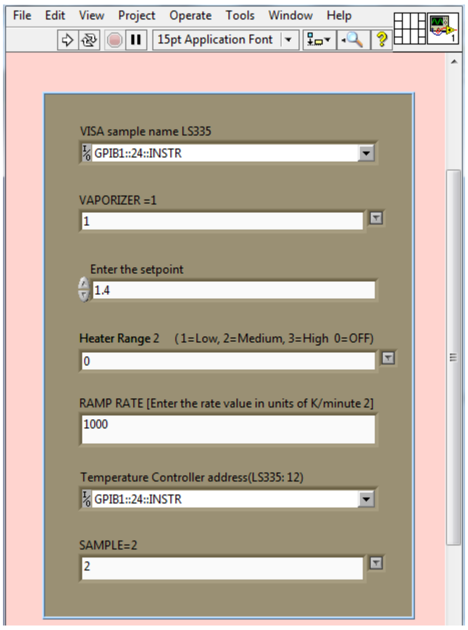

VISA sample name LS335: GPIB1::24::INSTR

VAPORIZER =1: 1

Enter the setpoint: 1.4

Heater Range 2 (1=Low, 2=Medium, 3=High 0=OFF): 0

RAMP RATE [Enter the rate value in units of K/minute 2]: 1000

Temperature Controller address(LS335: 12): GPIB1::24::INSTR

SAMPLE=2: 2

FIGURE 3.3: Front Panel of the temperature control program

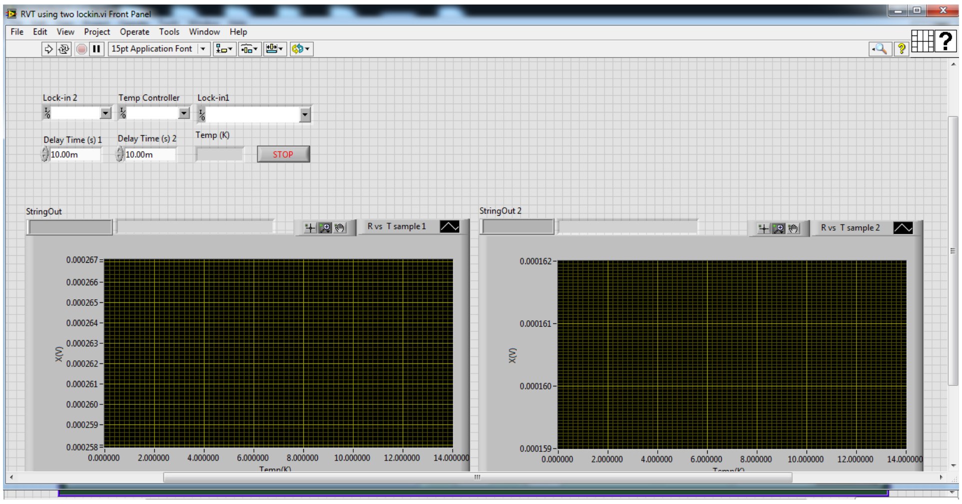

Delay Time (s) 1: 10.00m

Delay Time (s) 2: 10.00m

FIGURE 3.4: RT program for measuring resistance Vs Temperature of two samples simultaneously

3.2.3 The PCS Program

Point Contact Spectroscopy or the PCS program was written for the acquisition of the data while performing a PCS measurement. The program takes the sweep current range from the user and performs the spectroscopy. It plots the differential resistance(measured using lock-in) at Y-axis and the DC voltage(measured using digital multimeter) on the X-axis. The data hence acquired is saved in a separate text file. A pre-program was also written which was intended for setting the right parameter before starting the measurement. The program displays various values on screen and helps set values directly with on-screen commands. For example the signal recorded has to small(within 100μV) for the recording of the differential resistance. Using the pre-program(see Appendix E) such parameters can be easily set without accessing the instruments manually.

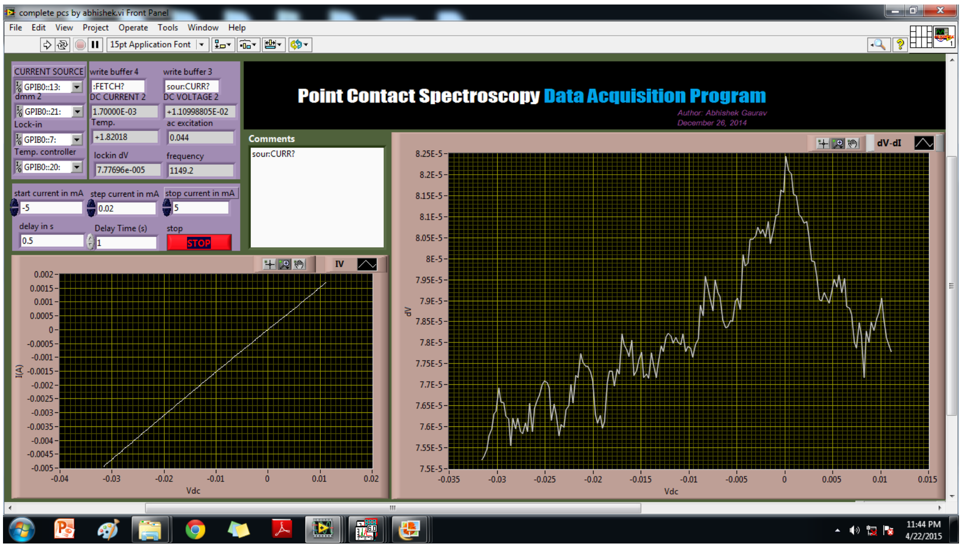

CURRENT SOURCE: GPIB0::13:
dmm 2: GPIB0::21:
Lock-in: GPIB0::7:
Temp. controller: GPIB0::20:
write buffer 4: :FETCH?
write buffer 3: sour:CURR?
DC CURRENT 2: 1.70000E-03
DC VOLTAGE 2: +1.10998805E-02
Temp.: +1.82018
ac excitation: 0.044
lockin dV: 7.77696e-005
frequency: 1149.2
start current in mA: -5
step current in mA: 0.02
stop current in mA: 5
delay in s: 0.5
Delay Time (s): 1
Comments: sour:CURR?

Figure 3.5: Front panel of the PCS program. The window on the right side plots the differential resistance(dV/dI) Vs. applied voltage(V) while the small window on the left plots the $I-V$ characteristic of the sample under measurement

Chapter 4

Unconventional Superconductivity at Mesoscopic Point-contacts on the 3-Dimensional Dirac Semi-metal Cd_3As_2

Cd_3As_2 being a 3D-DS is a potential candidate for the exhibiting novel phenomenon. Here we show that the emergence of unconventional superconductivity at the interface of this semi-metal and a normal metal like Ag, Pt, Au or ferromagnet like Fe and Co. Working with mostly the Ag-Cd_3As_2 point contact we establish the emergence of superconductivity and report the discovery of this unique phenomenon. However the phenomenon was later reported by other groups around the world as well.

In Figure 4.1 (a) we demonstrate a schematic diagram describing how the mesoscopic point-contacts between the metallic tips and Cd_3As_2 were formed *in-situ*. Current was sent through 1 and 4 and 2 and 3 were used to probe the voltage across the point contact. As mentioned in the earlier chapter the resistance of such a PC is dominated by Sharvin's or Maxwell's contribution depending on the regime it is in and in general is given by the Wexler's relation.[8]

$$R_{PC} = \frac{2h/e^2}{(ak_F)^2} + \Gamma(l/a)\frac{\rho(T)}{2a} \tag{4.1}$$

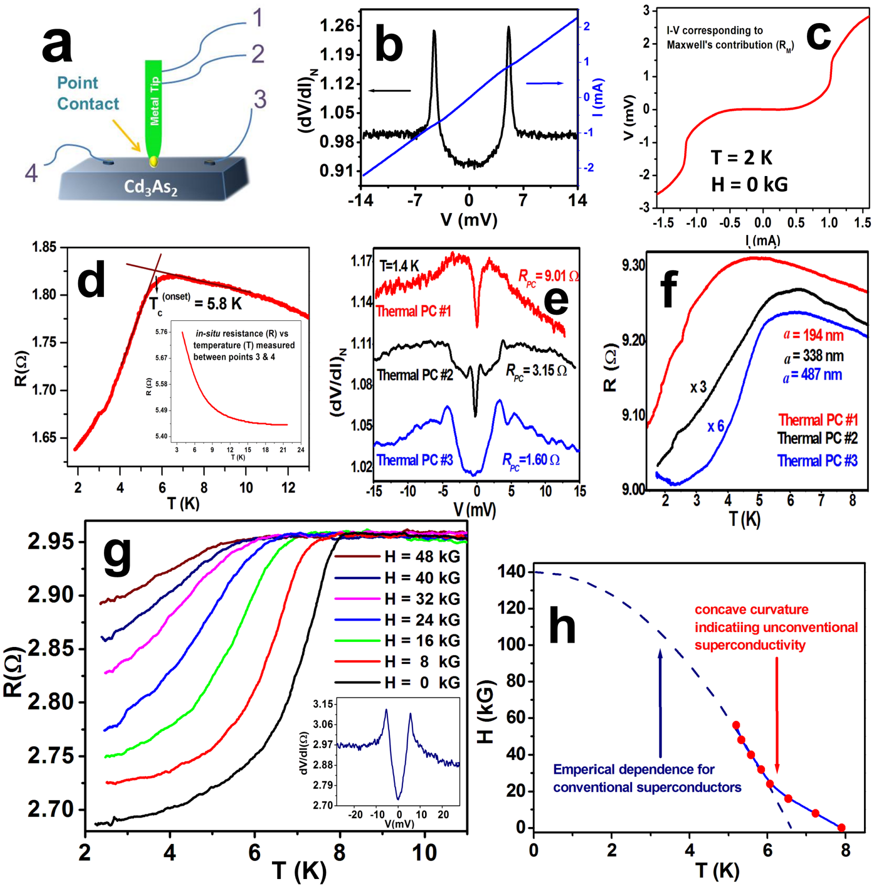

FIGURE 4.1: (a) The diagram representing the point-contact and the measurement electrodes. (b) A normalized differential resistance ($(dV/dI)_N$) spectrum close to the thermal regime: The peaks in $(dV/dI)_N$ originate due to the critical current of the superconducting junction. The blue line shows the $I - V$ corresponding to the total resistance ($R_M + R_S$) of the point-contact. (c) The I-V corresponding to R_M after subtracting R_S. This shows the dissipationless current flowing through the point-contact. (d) Resistance (R) of the point-contact as in (b) vs. temperature (T) showing the superconducting transition. The inset depicts the two probe resistance of the sample measured between the electrodes 3 and 4 *in-situ*. For 4-probe resistance see the chapter on "Materials and Characterization". (e) Additional spectra in the thermal regime showing the superconductivity-related features such as drop in differential resistance at lower voltage and the critical current driven peaks in $(dV/dI)_N$ and (f) R-T curves for corresponding point-contacts in (e) showing superconducting transition. (g) Magnetic field dependence of the R-T for a point-contact formed on a different sample with higher mobility (the in-field data have been given vertical shift to match the normal state resistance, see Supplementary Figure S10). The inset shows the corresponding dV/dI vs. V spectrum at zero field. (h) The $H - T$ phase diagram. The dotted line shows the emperical prediction for a conventional superconductor. The red dots are the data points extracted from the graphs in (g). The blue line is a guide to the eye.

where h is Planck's constant, e is the charge of a single electron, a is the contact diameter, $\Gamma(l/a)$ is a slowly varying function of the order of unity, ρ is the bulk resistivity of the material and T is the effective temperature at the point-contact. Two sharp peaks symmetric about $V = 0$ in dV/dI vs. V plots obtained from non-ballistic point-contacts is a known signature of superconductivity.[6, 12] The peaks appear when the dc-current flowing through the point-contact reaches the critical current for the given point-contact.[12] The measured normalized differential resistance ($(dV/dI)_N$) as a function of a dc-bias (V) developed across a point-contact between Ag and Cd_3As_2 is shown in Figure 4.1 (b). Two sharp peaks in $(dV/dI)_N$ are observed at $\pm 5mV$ respectively confirming that the point-contact is superconducting. The $I - V$ shown as a blue line in the figure corresponds to the total resistance of the point-contact ($R_{PC} = R_M + R_S$). We have separately calculated the $I - V$ corresponding to R_S using the theory of BTK for superconducting point-contacts[11] and subtracted the same from R_{PC}(see Appendix B for details). The resultant $I - V$ corresponding to R_M is shown in Figure 4.1(c) and it clearly shows the dissipationless state of the superconducting point-contact. We have also measured the resistance of the point-contact (R) as a function of temperature (T) by sending an ac-current through electrodes 1 and 4 and by measuring the ac-voltage drop between the electrodes 2 and 3. As shown in Figure 4.1(c), we clearly see the signature of a superconducting transition in the R-T plot. The onset of this transition is 6K. Since neither Cd_3As_2 nor Ag are superconductors it is rational to conclude that only a confined region at the interface between Ag and Cd_3As_2 becomes superconducting thereby giving rise to a novel state of matter.

We have repeated the measurements on more than 100 point-contacts on three samples (with different mobilities) grown in different batches. Some of the representative $(dV/dI)_N$ spectra are shown in Figure 4.1(d) and the corresponding R-T data are also shown in Figure 4.1(e). For all the point-contacts close to the thermal limit we observe the critical current driven peaks in $(dV/dI)_N$ and the position of the peaks are different for different contacts confirming the geometry dependence of the critical current. The size of the point-contacts that we have investigated varied between 20 nm and 450 nm(see Appendix D for details). No systematic dependence of the critical temperature on the contact size was found.

In order to further investigate the superconducting nature of the point-contacts we have performed magnetic field dependence of one of the point-contacts (Figure 4.1(g)) and constructed the $H - T$ phase diagram (Figure 4.1(h)). In Figure 4.1(h) we also show the emperical prediction as a dotted line for a conventional superconductor. The deviation of the measured data from the emperical prediction

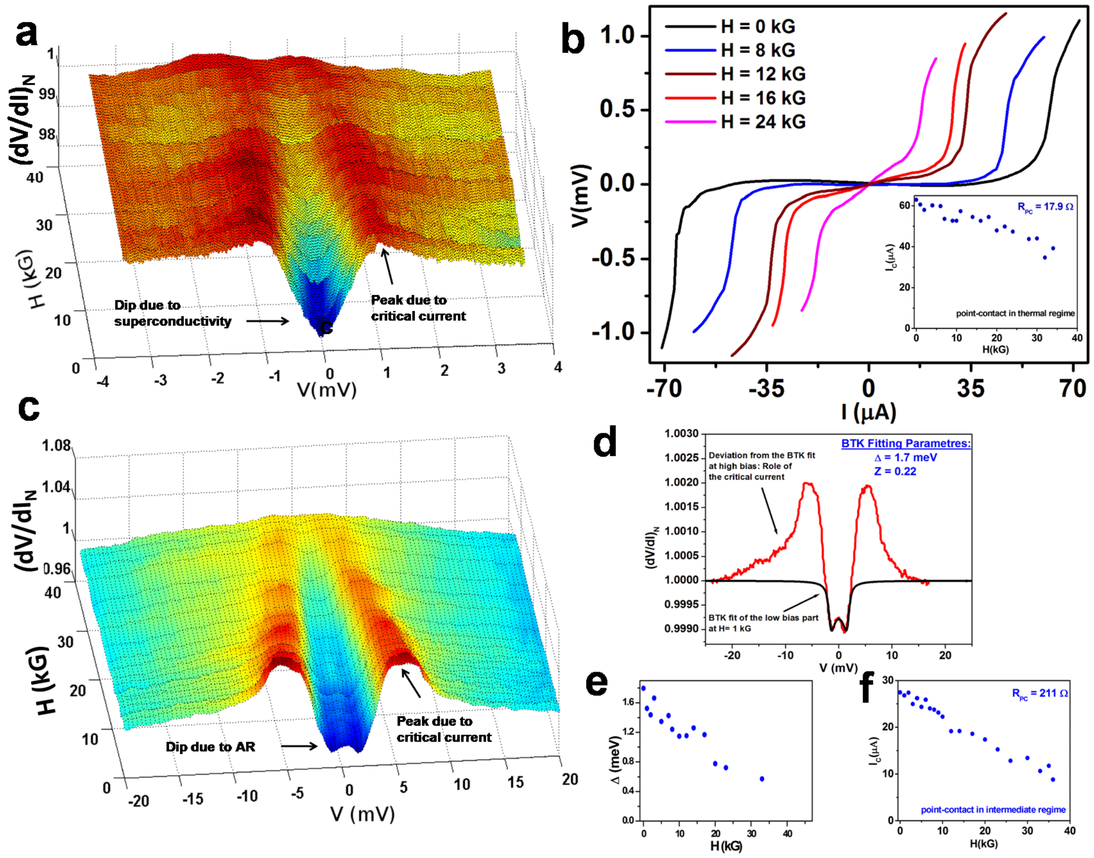

FIGURE 4.2: (a) The magnetic field dependence of a spectrum in the thermal regime. The peaks in normalized differential resistance ($(dV/dI)_N$) due to critical current of the superconducting point-contact are indicated by arrows. (b) Magnetic field dependence of the $I-V$ corresponding to R_M. the inset shows the magnetic field dependence of critical current (I_C) for the point-contact in the thermal regime. (c) The magnetic field dependence of a point-contact spectrum in the intermediate regime. The peaks in $(dV/dI)_N$ originating from critical current of the superconducting point-contact and the dips in $(dV/dI)_N$ originating from the Andreev reflection (AR) at the interface between Cd_3As_2 and Ag are indicated by arrows. (d) BTK fit to the low-bias portion of the intermediate regime spectrum(see Appendix C for details) obtained at 1 kG confirming Andreev reflection. The deviation from BTK at high bias is due to the role of critical current [12]. (e) Magnetic field dependence of the position of the AR dip (this is approximately equal to the gap Δ) and matches well with the Δ extracted from BTK fitting. However, it is known that in the non-ballistic limit the gap is always underestimated[12]). (f) Magnetic field dependence of the critical current for the spectrum in the intermediate regime as in (c).

at higher temperature with a concave curvature is a signature of unconventional superconductivity.[10]

In Figure 4.2(a) we show how the critical current dominated spectra obtained from the point-contacts close to the thermal limit evolve with magnetic field. The central dip (due to superconducting transition below the critical current) in the

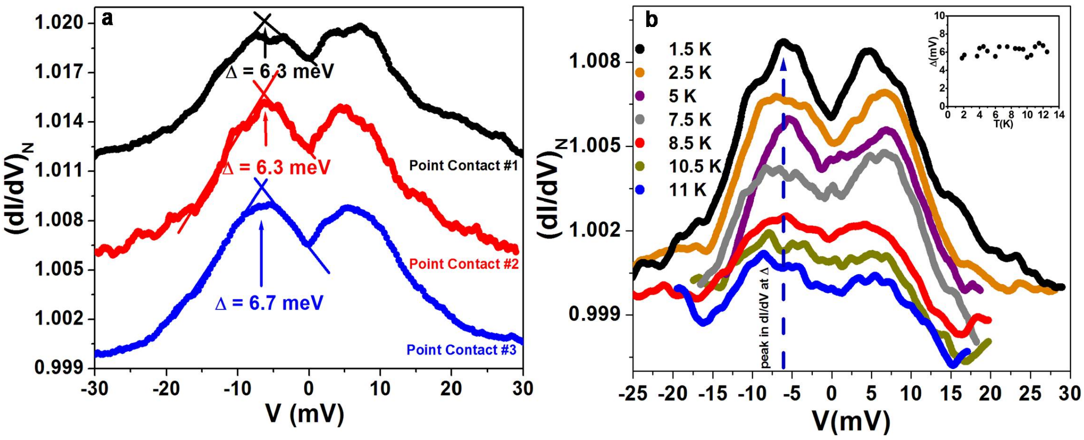

Figure 4.3: (a) Spectra captured from three point-contacts in the ballistic regime showing the gap (Δ) features. The spectra have been given a vertical shift for visual clarity. The scheme of computing Δ is also shown. (b) Temperature evolution of a spectrum showing the gap feature (Δ). *inset:* The temperature dependence of Δ. In this plot we show more data points than the number of spectra shown. Δ survives above 13 K which is more than 2 times T_c and does not show considerable temperature dependence indicating the presence of a pseudogap.

spectra evolves smoothly with magnetic field and disappears at $H_c = 4.5$ T. The critical-current driven side-peaks also show systematic evolution with magnetic field. The magnetic field dependence of the critical current dominated part of the $I-V$ characteristics (corresponding to R_M) is shown in Figure 4.2(b). The position of the peaks in dV/dI gives the approximate value of the critical current for a given point-contact (inset of Figure 4.2(b)). As expected for superconducting junctions, the critical current decreases with increasing magnetic field.

When the point-contacts are in the ballistic regime of transport, where the quasiparticles do not undergo in-elastic scattering within the contact region, it is possible to perform energy resolved Andreev reflection spectroscopy to determine the energy gaps.[11] As the tip is withdrawn from the sample slowly, the thermal regime point-contacts transition to a ballistic regime through an intermediate regime.[12] One representative spectrum in the intermediate regime is shown in Figure 4.2 (c). In the intermediate regime of transport, we have found signature of critical current driven features (peaks in $(dV/dI)_N$ symmetric about $V = 0$) as well as Andreev reflection driven features (dips in $(dV/dI)_N$ symmetric about $V = 0$) in the spectrum. In this case the gap-structure appears at a lower voltage due to the thermal contribution to the spectrum.[6, 12] A low-bias fit of the spectrum was possible using standard BTK theory[11] confirming the observation of Andreev reflection. Such analysis indicated a gap value of 1.8 meV (see supplementary information). The magnetic field dependence of the same spectrum is also shown in Figure 4.2(c) where it is seen that the critical current (I_c) decreases with increasing magnetic field (H) (Figure 4.2(d)). The magnetic field evolution of the gap structure (Figure 4.2(e)) shows that the gap decreases monotonically with increasing magnetic field.

Representative spectra obtained from three point-contacts in the ballistic regime are shown in Figure 4.3(a). The ballistic nature of such point-contacts were verified by measuring the temperature dependence of the normal state resistance that remained temperature independent. Two peaks symmetric about $V = 0$ appear in the differential conductance ($(dI/dV)_N$) vs. V spectra at 1.4 K – this feature is a hallmark of Andreev reflection with a finite potential barrier at a superconducting junction.[11] The peaks are significantly broader than what is expected from BTK theory that is traditionally used to analyze Andreev reflection spectra obtained on conventional BCS superconductors.[11] This might be due to a large inelastic broadening[13, 14] parameter at the interface and an unconventional pairing. Nevertheless, the position of the peaks provide an approximate estimate of the gap. [11] From the spectra provided in Figure 4.3(a) it is found that the magnitude of the gap in this case is approximately 6.5 meV. This value is unusually large given the low T_c (> 6 K) of the superconducting phase as that points to a dramatically large value for $\Delta/k_BT_c \sim 10$.

In order to obtain further insight about the gap feature observed at 1.4 K we have performed temperature dependence of the $(dI/dV)_N$ spectra in the ballistic regime (Figure 4.3(b)). Surprisingly, the position of the peak in $(dI/dV)_N$ does not show significant shift with increasing temperature and the peaks survive up to 13 K beyond which the spectra become flat due to thermal broadening. This observation is strikingly similar to the pseudo-gap feature observed in case of the cuprates where the peaks in $(dI/dV)_N$ representing the pseudogap do not shift with temperature.[15] It should also be noted that although the onset temperature of superconductivity is 6 K, the Andreev reflection like features are observed up to 13 K. Similar observation was made earlier in the context of the ferro-pnictide[16, 17] and the chalcogenide superconductors.[17] This was attributed to (1) Andreev reflection originating from pre-formed phase incoherent Cooper pairs[18] in the normal state of epitaxial thin films of ferropnictide superconductors[16] and (2) a novel phase of matter not related to superconductivity in the normal state of the

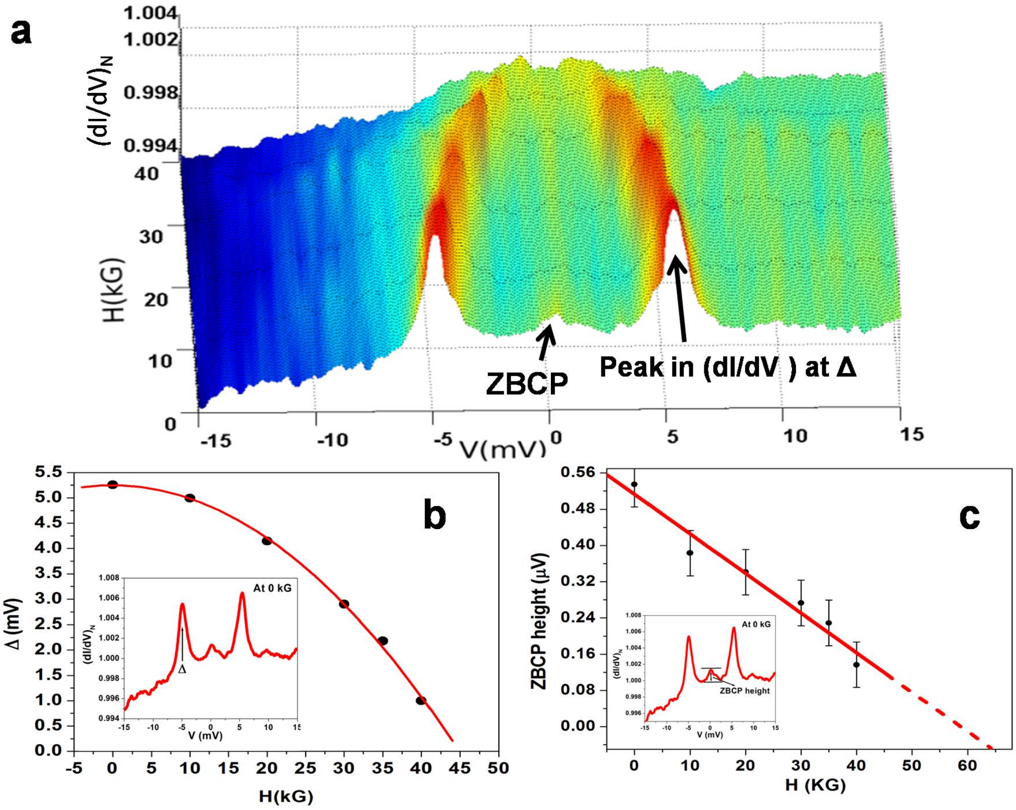

FIGURE 4.4: (a) The magnetic field evolution of a spectrum in the ballistic regime showing the gap feature as well as a prominent ZBCP. (b) The field evolution of estimated Δ. The inset shows the peak in $(dI/dV)_N$ corresponding to Δ. (c) The field dependence of the ZBCP height. The scheme followed for mesuring the ZBCP height is shown in the inset.

iron chalcogenide superconductors.[17] However, in the second case the spectral features exhibited a systematic temperature dependence unlike what we observe here.

In order to investigate the relation of this gap with superconductivity, we have probed the magnetic field dependence of the spectra obtained on a point-contact in the ballistic regime (Figure 4.4(a)). The gap features show systematic dependence on magnetic field and the extrapolation of this dependence indicates that the gap feature vanishes around 45 kG. Therefore, it is confirmed that in this case the pseudogap is a precursor phase to the superconducting state.

All the spectra obtained in the ballistic regime also show a peak structure in $(dI/dV)_N$ at $V = 0$. When the over-all signal is large, this structure is clearly visible. As shown in Figure 4.4(a), for certain point-contacts, this zero-bias conductance peak (ZBCP) is pronounced. Such a ZBCP is commonly seen for *ab*-plane tunneling in *d*-wave superconductors where it is attributed to the existence of zero energy Andreev Bound states (ABS).[19] However, as it is shown in Figure 4.4(c) it is observed that the ZBCP does not undergo splitting and slowly fades away with increasing magnetic field. This unique magnetic field dependence hints to the existence of Andreev bound states (ABS) due to a possible *p*-wave component in the order parameter symmetry of the new superconducting phase.[20] From the magnetic field dependence it is seen that the ABS is robust and survives up to a high magnetic field. Since the superconducting phase has been derived from a topologically non-trivial system, the robustness against applied large magnetic field might also indicate the existence of time-reversal-invariant Majorana edge-modes in the Cd_3As_2 point-contacts.[14, 21] In fact, such a ZBCP with similar magnetic field dependence was earlier observed in the topological superconductor $Cu_xBi_2Se_3$, where the ZBCP was attributed to the existence of Majorana Fermions.[22–25]

In conclusion, we have discovered an exotic unconventional superconducting phase at nano-meter scale interfaces between pure elemental metals and the 3-D Dirac semi-metal Cd_3As_2 with critical temperature more than 6 K. We also found evidence of a robust, temperature independent pseudogap up to 13 K. We found the signature of a ZBCP that could be the signature of topological superconductivity. The new phenomenon reported here is intriguing and therefore, this will motivate rigorous theoretical work. It is expected that following this work new devices involving the new 3-D topological Dirac semi-metals will be fabricated for exploring further intriguing phases of matter in confined dimensions. The superconducting phase presented here may be realized in nanostructured devices, interfaces, nanoparticles and nano-composites involving Cd_3As_2 and elemental normal metals like Ag, Au or Pt(refer to Appendix E).

Appendix A

Some frequently used commands for lock-in(model-SRS830), temperature controller(model-Lakeshore 350 and 335), digital multimeter(model-Keithley 2000) and the current source that were used.

lock-in commands

- OUTP? 1 - For recording the voltage(cosine component)
- AUXV1, 0- For setting the auxiliary voltage output(channel 1) to 0
- APHS - For autophasing the signal with the reference
- SLVL X-For setting the ac signal amplitude of the lockin to X(in Volts)

Temperature control commands

- KRDG?A - For reading the temperature in K when the sensor is connected to channel A

Current source commands

- SOUR:CURR X- For setting the current to X(in Amperes)
- OUTP ON- For turning the output of the current source on

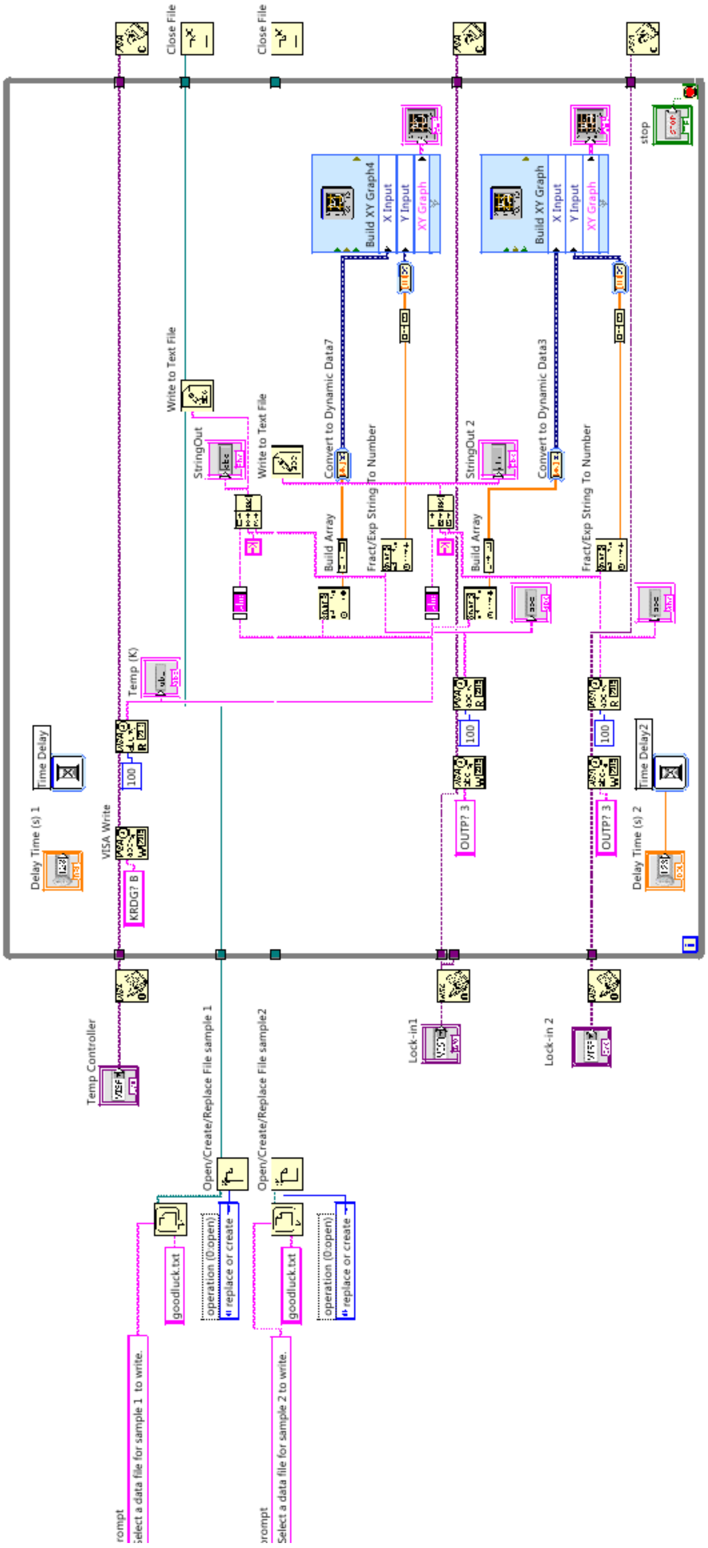

FIGURE A.1: The block diagram of the Labview program written for acquiring *RT* of two samples simultaneously

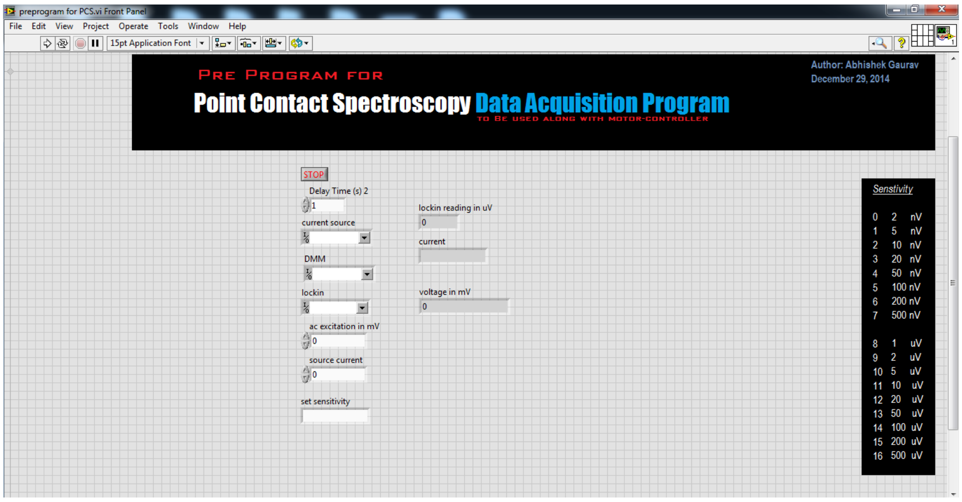

PRE PROGRAM FOR

Point Contact Spectroscopy Data Acquisition Program

TO BE USED ALONG WITH MOTOR-CONTROLLER

Author: Abhishek Gaurav
December 29, 2014

STOP

Delay Time (s) 2: 1

current source

DMM

lockin

ac excitation in mV: 0

source current: 0

set sensitivity

lockin reading in uV: 0

current

voltage in mV: 0

Senstivity

0	2	nV
1	5	nV
2	10	nV
3	20	nV
4	50	nV
5	100	nV
6	200	nV
7	500	nV
8	1	uV
9	2	uV
10	5	uV
11	10	uV
12	20	uV
13	50	uV
14	100	uV
15	200	uV
16	500	uV

FIGURE A.2: Pre-program for PCS intended for setting the right parameters before actually running the experiment

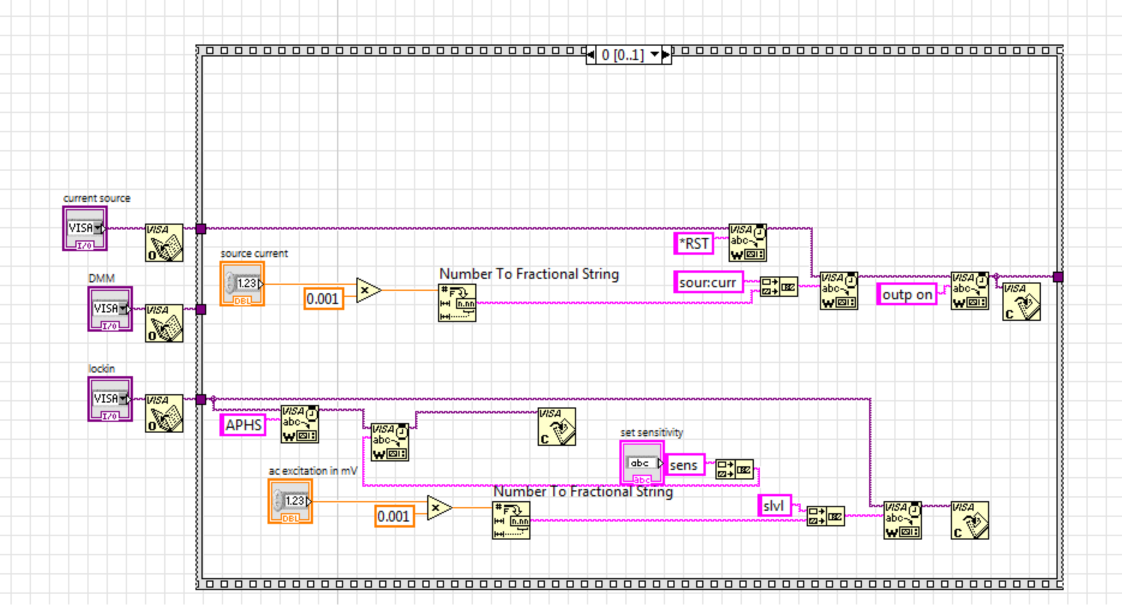

FIGURE A.3: Pre-PCS program block diagram

Appendix B

The following figure explains the dissipationless state that was shown in Figure 4.1(b).

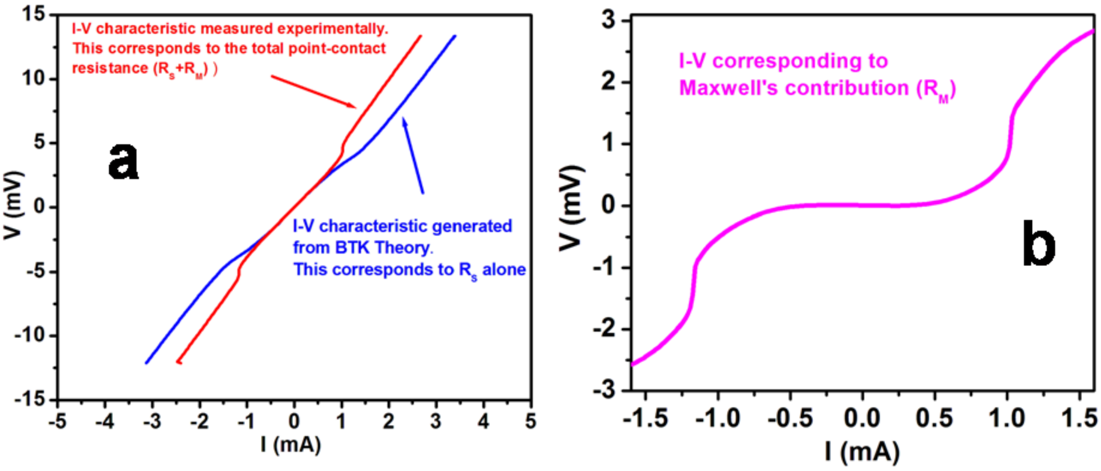

FIGURE B.1: The Sharvin's contribution(blue line) is substracted from the total resistance(red line) to show the dissipationless current in the superconducting state.

Appendix C

The size of the point contact was calculated following Wexler's formula. The normal resistance(at high bias) was taken as R_{PC}. $\Gamma(l/a)$ was taken to be unity. $2h/e^2$ is quantum resistance and equals $50k\Omega$. k_F is the magnitude of the Fermi wave vector which is 0.04Å for Cd_3As_2 and $\rho(T)$ is resistivity at temperature T(in K). $\rho(1.5) = 28$cm was used in the caluclation and was taken from the measured value of the four probe measurement on Cd_3As_2.

PC resistance(Ω)	Size(nm)
1.8	448
2.5	380
2.6	371
3.1	338
6.3	232
9	194
21	123
22	121
24	116
122	51
209	39

Table C.1: List of some of the PC size and their resistance

Appendix D

Fitting of dV/dI spectrum in the intermediate regime using BTK theory.

From the general shape of the dV/dI spectra it is clear that the intermediate regime data has contribution from both Andreev reflection and critical current. In order to confirm the existence of the Andreev reflection contribution, we have differentiated the expression of current ($I_{ballistic}$) with respect to V and compared the same with the experimental data. The representative fittings with the fitting parameters are shown in Figure C.1.

The data obtained in the ballistic regime are significantly broader than the BTK prediction. This is because in the ballistic regime the inealstic scattering processes are forbidden and therefore, the features associated with unconventional component of the order parameter are prominent.

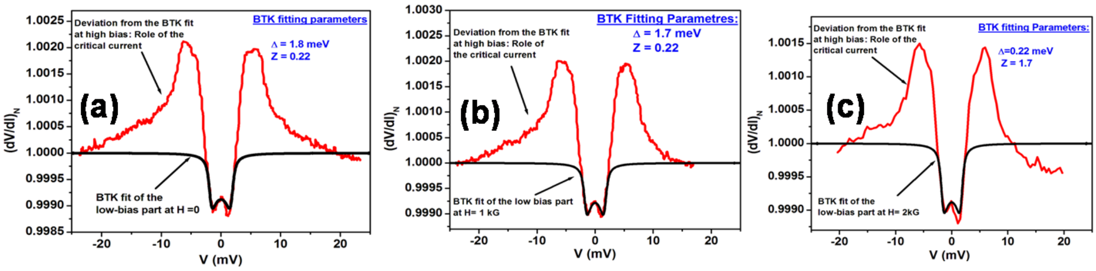

Figure D.1: Three Ag-Cd_3As_2 point-contact spectra obtained at different magnetic fields in the intermediate regime with low-bias BTK fits.

The fact that we could fit the low-bias part of the spectrum with BTK theory also confirms that the order parameter symmetry in the new superconducting phase is a mixed angular momentum symmetry with a strong s-wave component. From the analysis and discussion regarding the observed ZBCP presented in the main

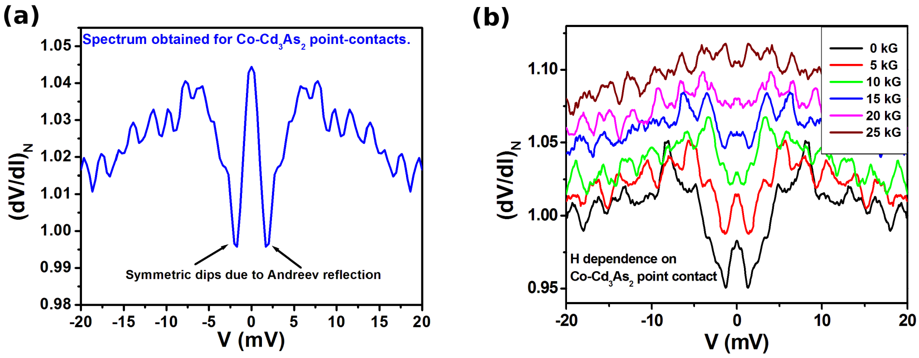

Figure D.2: Magnetic field dependence of normalized differential resistance spectrum obtained from a Co-Cd_3As_2 point-contact.

text there is a strong indication that a $s+p$-wave type of symmetry is possible in this new superconducting phase.[26]

The possible p-wave contribution is further supported by our experiments on the point-contacts made with a spin-polarized metal (Cobalt) where the Andreev reflection related features are clearly visible (see Figure C.2) indicating that the superconducting properties are not strongly suppressed by the proximity of a metal with spin-polarized Fermi-surface. Moreover, the superconductivity related features for the Co-Cd_3As_2 point-contacts survived up to a high magnetic field of 25 kG.

Appendix E

Different metallic and ferromagnetic tip showed the phenomena of this unconventional superconductivity described in detail in Chapter 4. The spectra given below shows the experiment done with Au, Pt , Fe and Co tips.

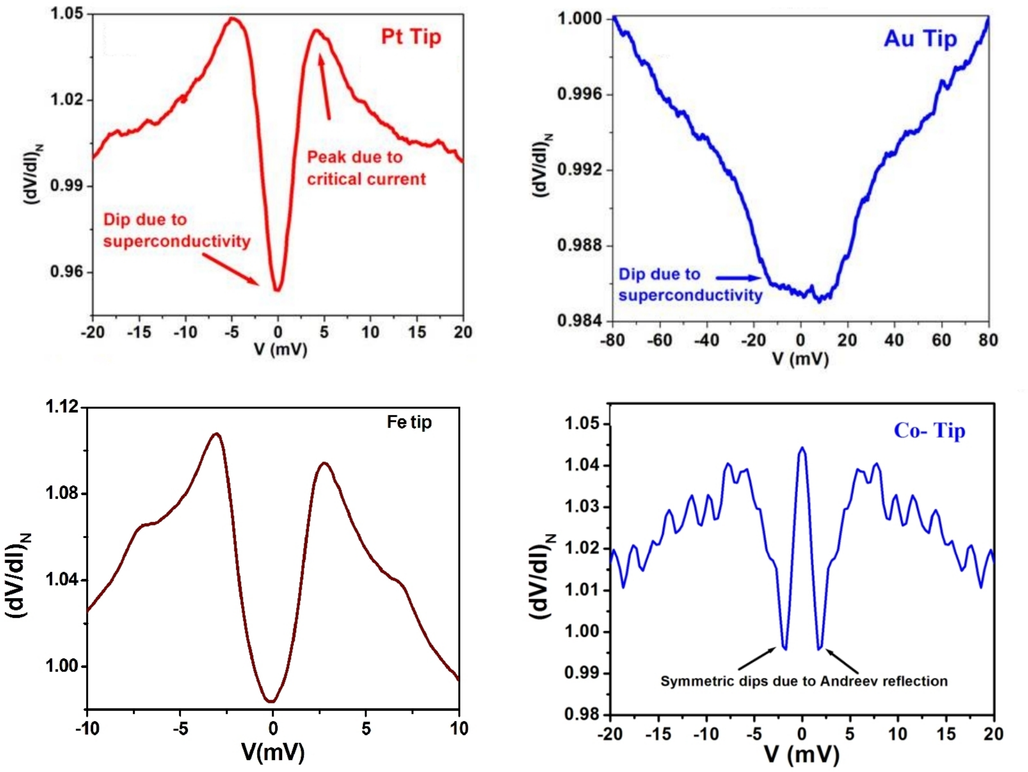

FIGURE E.1: Spectra of Cd_3As_2 with different metallic tips

Bibliography

[1] Hasan, M. Z. & Kane, C. L. Colloquium: Topological insulators. *Rev. Mod. Phys.* **82**, 3045-3067 (2010).

[2] Qi, X. -L. & Zhang, S. -C. Topological insulators and superconductors. *Rev. Mod. Phys.* **83**, 1057-1110 (2011).

[3] Gibson, Q. D. *et.al*. *arXiv* **1411.0005v1**, 31-Oct(2014).

[4] Liu, Z. K. *et.al*. Discovery of a three-dimensional topological Dirac semimetal, Na_3Bi. *Science* **343**, 864-867 (2014).

[5] Liu, Z. K. *et.al*. A stable three-dimensional topological Dirac semimetal $\mathrm{Cd_3As_2}$. *Nature Materials* **13**, 677-681 (2014).

[6] Naidyuk, Y. G. & Yanson, I. K. *Point-contact Spectroscopy.* Springer Newyork, 2004.

[7] Sharvin, Y.U *Sov.Phys.-JETP* **21**, 1965.

[8] Wexler, A. The size effect and the non-local Boltzmann transport equation in orifice and disk geometry. *Proc. Phys. Soc.* **89**, 927-941 (1966).

[9] Sheet, G. *Point-Contact Andreev Reflection Spectroscopy on Superconductors and Ferromagnets*,PhD Thesis, 2006.

[10] Tinkham, M. *Introduction to Superconductivity*, Second Edition, McGraw-Hill, Inc., 2004.

[11] Blonder, G. E., Tinkham, M. & Klapwijk, T. M. Transition from metallic to tunneling regimes in superconducting microconstrictions: excess current, charge imbalance, and supercurrent conversion. *Phys. Rev. B* **25**, 4515-4532 (1982).

[12] Sheet, G., Mukhopadhyay, S. & Raychaudhuri, P. Role of critical current on the point-contact Andreev reflection spectra between a normal metal and a superconductor. *Phys. Rev. B* **69**, 134507 (2004).

[13] Plecenk, A., Grajcar, M., Beaka, S., Seidel, P. & Pfuch, A. Finite-quasiparticle-lifetime effects in the differential conductance of $Bi_2Sr_2CaCu_2O_y/Au$ junctions. *Phys. Rev. B* **49**, 10016 (1994).

[14] Sato, M., Tanaka, Y., Yada, K. & Yokoyama, T. Topology of Andreev bound states with flat dispersion. *Phys. Rev. B* **83**, 224511 (2011).

[15] Renner, Ch., Revaz, B. Genoud, J. Y., Kadowaki, K. & Fischer, O. Pseudogap precursor of the superconducting gap in under- and overdoped $Bi_2Sr_2CaCu_2O_8$. *Phys. Rev. Lett.* **80**, 149-152 (1998).

[16] Sheet, G. *et.al.* Phase-Incoherent Superconducting Pairs in the Normal State of $Ba(Fe_{1-x}Co_x)_2As_2$. *Phys. Rev. Lett.* **105**, 167003 (2010).

[17] Arham, H. Z. *et.al.* Gap-like feature in the normal state of $X(Fe_{1-x}Co_x)_2As_2$, X = Ba, Sr and $Fe_{1+y}Te$ revealed by Point Contact Spectroscopy. *Journal of Physics: Conference Series.* **400**, 022001 (2012).

[18] Choi, H. Y., Bang, Y. & Campbell, D. K. Andreev reflections in the pseudogap state of cuprate superconductors. *Phys. Rev. B* **61**, 9748-9751 (2000).

[19] Tanaka, Y. & Kashiwaya, S. Theory of Tunneling Spectroscopy of d-Wave Superconductors. *Phys. Rev. Lett.* **74**, 3451 (1995).

[20] Tanaka, Y., Tanuma, Y., Kuroki, K. & Kashiwaya, S. Theory of Magnetotunneling Spectroscopy in Spin Triplet p-Wave Superconductors. *J. Phys. Soc. Jpn.* **71**, 2102 (2002).

[21] Tanaka, Y., Sato, M. & Nagaosa, N. Symmetry and topology in superconductors- odd- frequency pairing and edge states. *J. Phys. Soc. Jpn.* **81**, 011013 (2012).

[22] Sasaki, S. *et.al.* Topological superconductivity in $Cu_xBi_2Se_3$. *Phys. Rev. Lett.* **107**, 217001 (2011).

[23] Takami, S. *et.al.* Quasi-Classical Theory of Tunneling Spectroscopy in Superconducting Topological Insulator. *J. Phys. Soc. Japan* **83**, 064705 (2014).

[24] Yamakage, A., Yada, K., Sato, M. & Tanaka, Y. Theory of tunneling conductance and surface-state transition in superconducting topological insulators. *Phys. Rev. B* **85**, 180509 (2012).

[25] Yamakage, A., Yada K., Sato M. & Tanaka Y. Theory of tunneling conductance and surface-state transition in superconducting topological insulators. *Phys. Rev. B* **85**, 180509(R) (2012).

[26] Kashiwaya, S. & Tanaka, Y. Tunnelling effects on surface bound states in unconventional superconductors. *Rep. Prog. Phys.***63**, 1641 (1999).